Anal Bioanal Chem (2016) 408:7193–7202
DOI 10.1007/s00216-016-9856-6

RESEARCH PAPER

A novel solid-state electrochemiluminescence sensor for detection of cytochrome *c* based on ceria nanoparticles decorated with reduced graphene oxide nanocomposite

Mohammad Reza Karimi Pur[3] · Morteza Hosseini[1,2] · Farnoush Faridbod[3] · Amin Shiralizadeh Dezfuli[3] · Mohammad Reza Ganjali[3,4]

Received: 13 May 2016 / Revised: 15 July 2016 / Accepted: 1 August 2016 / Published online: 24 August 2016

Abstract A novel ultrasensitive sensing system for the rapid detection of cytochrome *c* (Cyt C) was developed on the basis of an electrochemiluminescence (ECL) method. A nanocomposite biosensor was made of reduced graphene oxide decorated with cerium oxide/tris(2,2-bipyridyl)ruthenium(II)/chitosan (CeO_2NPs-RGO/ $Ru(bpy)_3^{2+}$/CHIT) and used for this purpose. The ECL signal was produced by an electrochemical interaction between $Ru(bpy)_3^{2+}$ and tripropyl amine (TPA) on the surface of the electrode. Addition of Cyt C to the solution decreases the ECL signal due to its affinity for TPA and inhibition of its reaction with $Ru(bpy)_3^{2+}$. The effects of the amount of CeO_2NPs-RGO, $Ru(bpy)_3^{2+}$, TPA concentration as a co-reactant, and the pH of the electrolyte solution on the ECL signal intensity were studied and optimized. The results showed that the method was fast, reproducible, sensitive, and stable for the detection of Cyt C. The method has a linear range from 2.5 nM to 2 μM ($R^2 = 0.995$) with a detection limit of 0.7 nM. Finally, the proposed biosensor was used for the determination of Cyt C in human serum samples with RSDs of 1.8–3.6 %. The results demonstrate that this solid-state ECL quenching biosensor has high sensitivity, selectivity, and good stability.

Keywords Electrochemiluminescence · Cerium oxide · Reduced graphene · Biosensor

Published in the topical collection *Analytical Electrochemiluminescence* with guest editors Hua Cui, Francesco Paolucci, Neso Sojic, and Guobao Xu.

Electronic supplementary material The online version of this article (doi:10.1007/s00216-016-9856-6) contains supplementary material, which is available to authorized users.

✉ Morteza Hosseini
smhosseini@khayam.ut.ac.ir

[1] Department of Life Science Engineering, Faculty of New Sciences & Technologies, University of Tehran, 16th Azar Avenue, Enghelab Square, 1417466191 Tehran, Iran

[2] Medical Biomaterials Research Center, Tehran University of Medical Sciences, 16th Azar Avenue, Enghelab Square, 1417466191 Tehran, Iran

[3] Center of Excellence in Electrochemistry, Faculty of Chemistry, University of Tehran, 1417466191 Tehran, Iran

[4] Biosensor Research Center, Endocrinology & Metabolism Molecular-Cellular Sciences Institute, Tehran University of Medical Sciences, 1417466191 Tehran, Iran

Introduction

Cytochrome *c* (Cyt C) is a vital heme-containing metalloprotein which is located in the intermembrane space of mitochondria. It acts as an electron transport between complex III and complex IV of the breathing chain. Cyt C is the key biomolecule in the electron transport chain and is also an intermediate species in apoptosis. When mitochondria are damaged under pathological conditions, Cyt C enters the cytosol of the cell. This release of Cyt C from mitochondria into the cytosol is a critical event in the activation of intracellular signaling and causes caspase activation and leads to programmed cell death (apoptosis). Cytochrome *c* which is released from the mitochondria into the cytosol can be a trigger of the apoptosis. In a review article in 2008, Brown and Borutaite explained that the oxidized form of cytochrome *c* (Fe^{3+}) can induce caspase activation via the apoptosome, while the reduced form (Fe^{2+}) cannot; however, it is unclear whether this difference in behavior is entirely due to the oxidized and reduced forms of cytochrome *c* or not. Cytosolic cytochrome *c* of healthy cells is rapidly reduced by various enzymes or reductant species and this blocks the apoptosis.

Whereas, in apoptotic cells, the oxidized cytosolic cytochrome *c* is rapidly oxidized by mitochondrial cytochrome oxidase and accessible due to permeabilization of the outer membrane. Thus, regulation of the redox state of cytochrome *c* potentially enables regulation of the intrinsic pathway of apoptosis [1, 2].

Therefore, monitoring of Cyt C is of great significance in clinical diagnostics and therapeutic research. The determination of Cyt C release was used for the screening of anticancer drugs, too [3]. Study of Cyt C redox activity was successfully used in the detection of respiratory poisons [4]. Recently, the analysis of Cyt C has attracted considerable attention and some techniques including cyclic voltammetry [5, 6], electrochemical impedance spectroscopy [7, 8], fluorescence spectrophotometry [9–12], and electrochemiluminescence [10, 13] have been reported for Cyt C measurement.

Electrochemiluminescence (ECL) is a well-known process in which the species generated at electrodes undergo high-energy electron transfer reactions to form excited states that emit light [14]. Because the ECL method shows some remarkable features such as low background, high sensitivity, good temporal/spatial control, low detection limit, and wide dynamic range, it has attracted much attention in recent years and is used extensively for biosensing purposes [15].

A solid-state ECL sensor based on the immobilization of tris(2,2-bipyridyl)ruthenium(II) ($Ru(bpy)_3^{2+}$) on the solid electrode surface can significantly reduce the use of expensive reagents, enhances the ECL signal, simplifies experimental design, and improves the detection sensitivity [16]. $Ru(bpy)_3^{2+}$ is widely used as a reagent in designing ECL sensors for a variety of analytes owing to its high emission efficiency, good stability in different pH, and superior electrochemical reversibility [17].

Use of nanomaterials in designing sensors is the most direct and simple strategy for signal amplification, because of their remarkable biocompatibility, conductivity, and the high loading of signal molecules for synergistic amplification of the target response [18–20]. Graphene (G), an allotrope of carbon in the form of a densely packed honeycomb two-dimensional lattice, has generated tremendous interest since its discovery in 2004 [21]. Graphene compounds are used in a wide variety of applications in the fields of photoelectric devices, fuel cells, sensors, and biosensors owing to their unique properties, such as high mechanical strength, good biocompatibility, high surface area, fast electron transfer rate, and potentially low manufacturing cost [22]. Recently, use of reduced graphene oxide (RGO) in construction of biosensors has been extensively studied [23]. Peng et al. indicated that nanocomposite RGO enhanced electrochemiluminescence of peroxydisulfate and provided a novel sensing strategy for biomolecules [24]. Zhou et al. fabricated graphene-Fe_3O_4 composite-modified indium tin oxide (ITO) electrodes to construct H_2O_2 biosensors [25]. These results indicate that RGO shows great potential as an amplification material in the fabrication of ECL biosensors.

Ceria (CeO_2), an oxide of cerium, has received great attention for its unique catalytic properties in redox reactions [26]. It has two common oxidation states, Ce^{3+} and Ce^{4+}, that make it a suitable compound for catalytic or electrocatalytic reactions. Also, owing to the high surface-to-volume ratio, CeO_2 has a high capacity to absorb molecules such as proteins, amino acids, and sugars [27].

Decoration of RGO with various nanoparticles produces a new class of hybrid materials with properties that are different from those of each individual component. For example, several metal oxides, such as SnO_2, Fe_3O_4, ZnO, TiO_2, Co_3O_4, and MnO_2, have been decorated on RGO for a variety of applications in energy storage, catalysis, and chemical and biosensing [28–32].

In this work, we constructed a new sensitive solid-state ECL nanocomposite biosensor for detection of Cyt C. The CeO_2 NPs-RGO/ $Ru(bpy)_3^{2+}$/chitosan (CHIT) modified glassy carbon electrode was designed to provide a large specific surface area and fast electron transfer rate enhanced ECL intensity. This ECL biosensor has a lower detection limit for cytochrome *c* in comparison with previously reported sensors.

Experimental

Materials and reagents

All the chemicals were of analytical reagent grade and used as received without further purification. Graphite powder (99.995 %), sulfuric acid (95 %), potassium permanganate, potassium nitrate, $Ce(NO_3)_3{\cdot}6H_2O$, aqueous NH_4OH, and N_2H_4 were purchased from Shanghai, China. Tris(2,2-bipyridyl)ruthenium(II) ($Ru(bpy)_3^{2+}$) chloride hexahydrate and chitosan were obtained from Sigma and used without further purification. Cytochrome *c* (bovine heart, molecular weight 12,588) and bovine serum albumin (98 %) were purchased from Sigma (St. Louis, MO, USA). Phosphate buffer solutions (PBS) with pH 7.4 were prepared by mixing K_2HPO_4, NaH_2PO_4, and KCl and adjusting the pH.

Apparatus

Cyclic voltammetry (CV) was performed using a PalmSens PC potentiostat–galvanostat (PalmSens, Houten, the Netherlands) with a conventional three-electrode setup in which a modified glassy carbon electrode, an Ag|AgCl|KCl sat. electrode, and a platinum wire served as the working, reference, and auxiliary electrodes, respectively. Electrochemical and ECL measurements were carried out in a 4-mL quartz cell. The working electrode was placed in an equatorial position in a quartz cell with its surface exactly in

front of the window of the Fl-win lab photomultiplier LS 50 (Perkin-Elmer) and fixed on a holder. The detector and ECL cell were enclosed in a light-tight black box. Electrochemical impedance measurements were carried out on AUTOLAB PGSTAT 30. The size and morphology of the nanoparticles were measured by scanning electron microscopy (SEM) using a KYKY-EM 3200 digital scanning electron microscope (China).

Preparation of CeO_2NPs -RGO nanocomposite

The CeO_2NPs-RGO nanocomposite was prepared according to a simple sonochemical method previously reported [29]. The procedure was briefly as follows. Initially, 1 mmol of $Ce(NO_3)_3{\cdot}6H_2O$ was dissolved in deionized water (30 mL). Then, during the ultrasound irradiation (in an ultrasonic bath), a 32 % NH_4OH aqueous solution (2 mL) was added dropwise to the solution. The process was completed within 66 min. Next, 60 mL aqueous solution of GO suspension (0.5 mg mL^{-1}), was added to the suspension and heated to 90 °C. Then 3 mL N_2H_4 was added and the suspension solution was heated at reflux for about 1 h. The resulting precipitate was washed several times with ethanol and distilled water before drying at 60 °C for 24 h. The final obtained product was CeO_2NPs-RGO.

Fabrication of ECL biosensor

A glassy carbon electrode (GCE) was polished well with 1.0, 0.3, and 0.05 μm alumina slurry on a polishing cloth, rinsed thoroughly with water, and sonicated in ethanol and then distilled water. A 100-μL aliquot of 2.5×10^{-3} mol L^{-1} $Ru(bpy)_3^{2+}$ aqueous solution was dispersed in 600 μL solution of 0.5 wt% chitosan which was prepared by dispersing 50.0 mg of chitosan in 10.0 mL of 3 % acetic acid. The CeO_2NPs-RGO/ $Ru(bpy)_3^{2+}$/ CHIT modified electrode was prepared by casting 4 μl of CeO_2NPs-RGO nanocomposite suspension (0.5 mg mL^{-1} and 1:2 mass ratio of CeO_2/G) on the electrode surface and dried at room temperature. Then, 5 μl of $Ru(bpy)_3^{2+}$/ CHIT suspension was dropped on the CeO_2NPs-RGO/GCE surface and dried at room temperature (Scheme 1).

Results and discussion

Characterization of CeO_2NPs-RGO

The crystal phase of the used CeO_2NPs-RGO nanocomposite was studied by x-ray diffraction (XRD). As shown in Fig. 1, the diffraction peaks at 28.58, 33.17, 47.50, 56.41, 59.14, 69.49, 76.80, 79.21, and 88.38, correspond to (111), (200), (220), (311), (322), (400), (331), (420), and (422) planes, respectively. The obtained pattern matches with a typical cubic fluorite-type structure of CeO_2 (JCPDS no. 34-0394), indicating that CeO_2 nanoparticles were successfully anchored on the RGO [33].

The FE-SEM image of the CeO_2 nanoparticles before and after combining with RGO is shown in Fig. 2. As can be seen, a large number of CeO_2 NPs were well dispersed on the RGO surface, indicating a good combination between nanoparticles and RGO. Through this combination, the agglomeration of CeO_2 nanoparticles can be prevented effectively. And on the other hand, the CeO_2 nanoparticles on the RGO's surfaces can act as spacers and prevent the RGOs from restacking [29]. Consequently, the new nanostructure can increase the stability of the RGO and provide a much more active surface area [34, 35].

Electrochemical and ECL signal

The catalytic effect of rare earth oxide NPs such as Sm_2O_3 [36], CeO_2 [37–39], and CeO_2–graphene [27] on the ECL reaction has been shown in previous studies. To study the effect of the CeO_2NPs-RGO nanocomposite on the oxidation of $Ru(bpy)_3^{2+}$ and corresponding ECL signal, cyclic voltammetry using $Fe(CN)_6^{3-}/Fe(CN)_6^{4-}$as redox probe and ECL potential study by the modified electrodes was performed in the potential range between 0.0 and 1.5 V vs. Ag|AgCl|KCl sat. at a scan rate of 100 mV s^{-1}. Figure 3A shows the CV curves for probing the electrode modification process. A redox peak of $Fe(CN)_6^{3-}/Fe(CN)_6^{4-}$was observed at the bare GCE (curve a). When CeO_2NPs-RGO-CHIT nanocomposites were coated on the electrode, the peak current markedly increased as a result of the increase in the electrode surface area and the excellent conductivity of CeO_2NPs-RGO nanocomposites (curve b). The peak current decreased in the absence of nanocomposites and the presence of Ru-CHIT (curve c). However, when CeO_2NPs-RGO added to Ru-CHIT, the peak current increased significantly (curve d). To investigate the effect of CeO_2NPs and RGO, two nanocomposites RGO -Ru-CHIT (curve e) and CeO_2NPs -Ru-CHIT (curve f) were also examinated. As shown in Fig. 3, the RGO-Ru-CHIT nanocomposites increased the peak current more than CeO_2 -Ru-CHIT.

Figure 3B presents the ECL–potential curves of the bare GCE and CeO_2-RGO-CHIT, Ru-CHIT, CeO_2-RGO-Ru-CHIT modified GCE (curves a–d). Clearly, bare GCE and CeO_2-RGO-CHIT modified electrode have negligible ECL emission (Fig. 3a,b). However, Ru- CHIT and CeO_2-RGO-Ru-CHIT modified GCE show high ECL intensity (Fig. 3c,d). It can be concluded that electrodes without $Ru(bpy)_3^{2+}$ are not able to produce ECL emission. Figure 3b shows that ECL emission of CeO_2-RGO-Ru-CHI modified electrode (curve d) compared with Ru-CHIT-GCE (curve c) increased twofold by modification of the electrode with CeO_2-

Scheme 1 Fabrication of ECL sensor

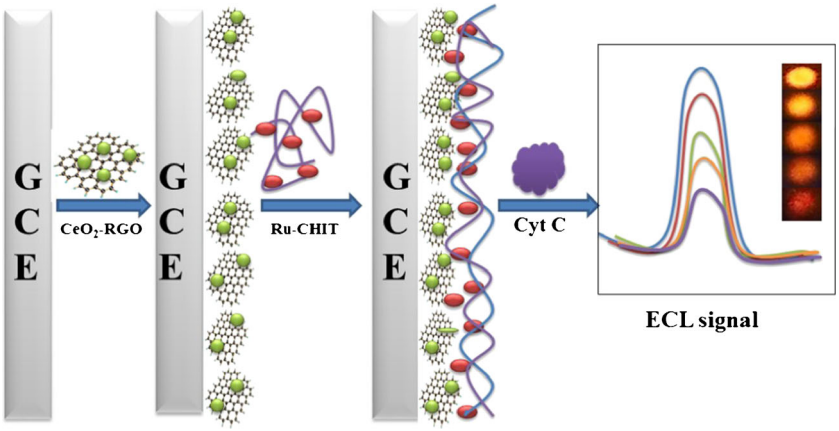

RGO nanocomposite. Also ECL emission of CeO_2NPs -Ru-CHIT (curve f) was higher compared with RGO -Ru-CHIT (curve e).This increase of ECL emission is attributed to the increase in the electrode surface area due to the presence of CeO_2-RGO nanocomposite and excellent electrical conductivity of the nanocomposite film [33]. In addition, CeO_2 NP decorated RGO can enhance the signal owing to the electrocatalytic activity. The redox behavior of Ce^{4+}/Ce^{3+} in the CeO_2 and Ce_2O_3 can significantly catalyze the oxidation of $Ru(bpy)_3^{2+}$ to $Ru(bpy)_3^{3+}$[37].

Electrochemical impedance spectroscopy (EIS) was employed to investigate the conductivity of the electrode surface due to the modification with CeO_2-RGO nanocomposite. Figure 4 shows the Nyquist plots of bare GCE, $Ru(bpy)_3^{2+}$-CHIT, and CeO_2 NP-RGO-$Ru(bpy)_3^{2+}$-CHIT in 0.1 M KCl solution with 5 mM $K_3Fe(CN)_6/K_4Fe(CN)_6$ electroactive probes. In the high frequency zone, the semicircle's diameter represents the electron-transfer resistance (R_{et}) of the electrochemical reaction, and the linear part of Z_{Im} versus Z_{Re} at lower frequencies represents diffusion-controlled electrode process. The EIS spectrum for the bare GCE exhibited a small semicircular domain, at high frequencies (Fig. 4, curve a), and its electron-transfer resistance (R_{et}) is small, indicating a fast electron-transfer process of $Fe(CN)_6]^{3-/4-}$. The spectrum for the $Ru(bpy)_3^{2+}$-CHIT electrode indicated much increased electron-transfer resistance (Fig. 4, curve b). After modification of the electrode with CeO_2 NP-RGO-$Ru(bpy)_3^{2+}$-CHIT, the semicircle diameter was much smaller, indicating a lower R_{et} value for $Fe(CN)_6]^{3-/4-}$ (Fig. 4, curve c). This showed that the CeO_2 NP-RGO nanocomposite could increase the conductivity of the electrode surface.

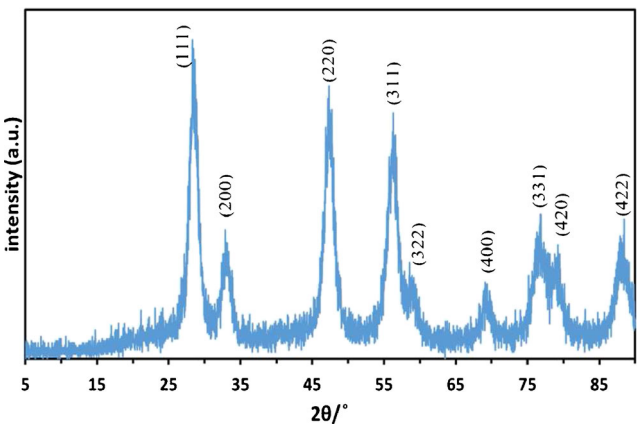

Fig. 1 XRD pattern of CeO_2 NPs-RGO

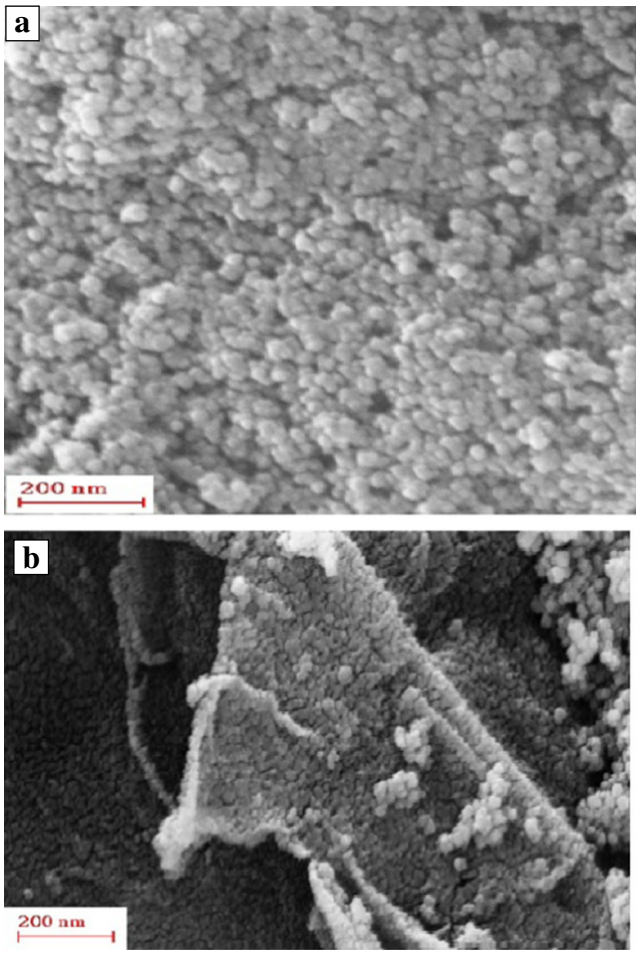

Fig. 2 SEM image of CeO_2 NPs before (**a**) and after combining with RGO (**b**)

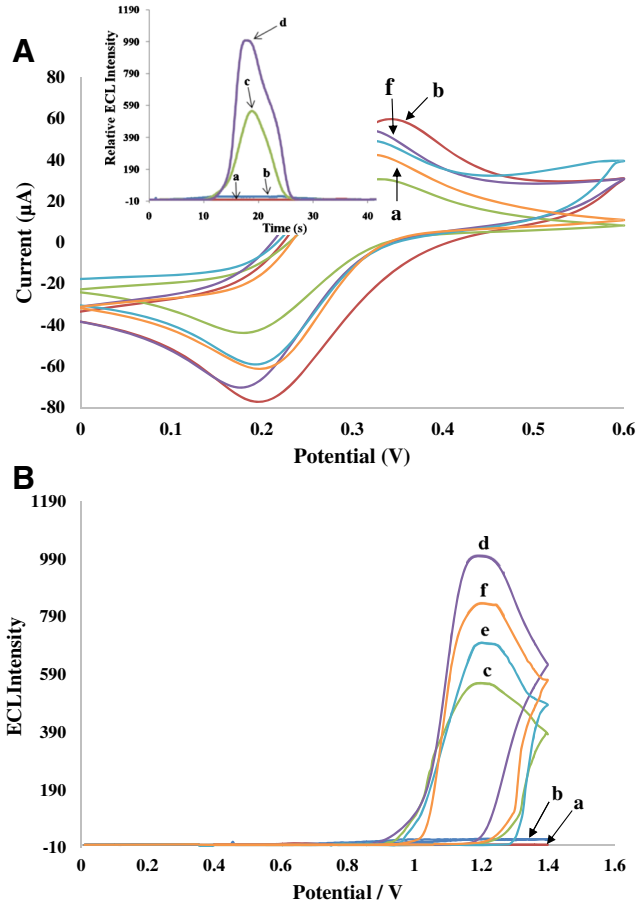

Fig. 3 CV (**A**) and ECL signal (**B**) from **a** bare GCE, **b** CeO_2-RGO-CHIT, **c** Ru-CHIT, **d** CeO_2-RGO/ $Ru(bpy)_3^{2+}$-CHIT, **e** RGO/ $Ru(bpy)_3^{2+}$-CHIT, **f** CeO_2/ $Ru(bpy)_3^{2+}$-CHIT. CV in 10 mM $Fe(CN)_6^{3-}$/$Fe(CN)_6^{4-}$(1:1) containing 0.1 M KCl. The CVs proceeded between 0 and 0.6 V with a scan rate of 100 mV s^{-1}. ECL curves in 0.1 M pH 7.4 phosphate buffer solution containing 0.5 mM TPA

Optimization of ESL signal

To optimize the performance of the proposed ECL biosensor towards cytochrome *c* detection, the effects of pH, concentration of CeO_2-RGO on the electrode surface, concentration of $Ru(bpy)_3^{2+}$, concentration of TPA, and scan rate on the intensity of ECL signal were investigated.

The relationship between the ECL intensity and pH was investigated over a pH range of 5.5 to 10. Figure S1 (A) in the Electronic Supplementary Material (ESM) shows that the ECL intensity increased considerably with the increase in pH value from 5.5 to 7.4 and then decreased. The maximum ECL intensity was observed at pH 7.4. Thus, phosphate buffer solution of pH 7.4 was chosen for further ECL biosensor determination.

The effect of CeO_2-RGO concentration on the electrode response of the ECL signal was investigated. As shown in ESM Fig. S1 (B), the ECL signal increased correspondingly when the concentration of CeO_2-RGO increased from 0.1 to 0.5 mg mL^{-1}, since the CeO_2-RGO promoted the electron transfer on the electrode surface. However, the ECL response decreased when the concentration of the CeO_2-RGO was more than 0.5 mg mL^{-1} is because of the blackbody effect. High ECL response was obtained at 0.5 mg mL^{-1} because there is a balance between the promoted charge transfer and the blackbody effect [40].

The effect of the $Ru(bpy)_3^{2+}$ concentration in the modified electrode on the intensity of the ECL signal was also investigated. As shown in ESM Fig. S1 (C) the ECL intensity increased with increasing $Ru(bpy)_3^{2+}$ concentrations. The intensity of the ECL signal in the presence of TPA increased linearly with an increase in the concentration of $Ru(bpy)_3^{2+}$ from 0.5 to 2.5 mM. However, further increase in the concentration of $Ru(bpy)_3^{2+}$ (up to 2.5 mM) did not cause any further enhancement in the intensity of the ECL signal (Scheme 2). Therefore, 2.5 mM was selected as the optimum concentration of $Ru(bpy)_3^{2+}$ in modified the ECL biosensor for detection of cytochrome *c*.

Figure S1 (D) in the ESM shows the relationship between ECL intensity and TPA concentration at modified electrodes. The ECL intensity was directly related to the TPA

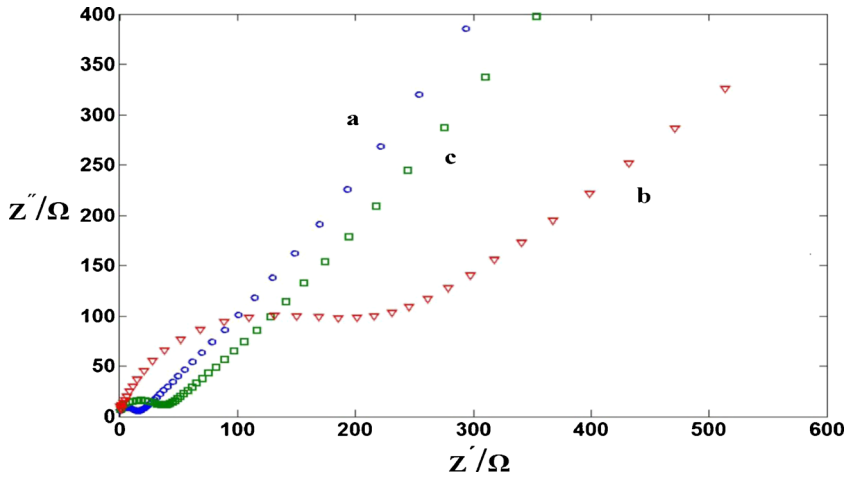

Fig. 4 Impedance of *a* bare GCE, *b* $Ru(bpy)_3^{2+}$-CHIT, *c* CeO_2-RGO/ $Ru(bpy)_3^{2+}$-CHIT in 10 mM $Fe(CN)_6^{-3/-4}$ in 0.1 M KCl solution in the frequency range of 0.01 Hz to 100 kHz and signal amplitude 5 mV

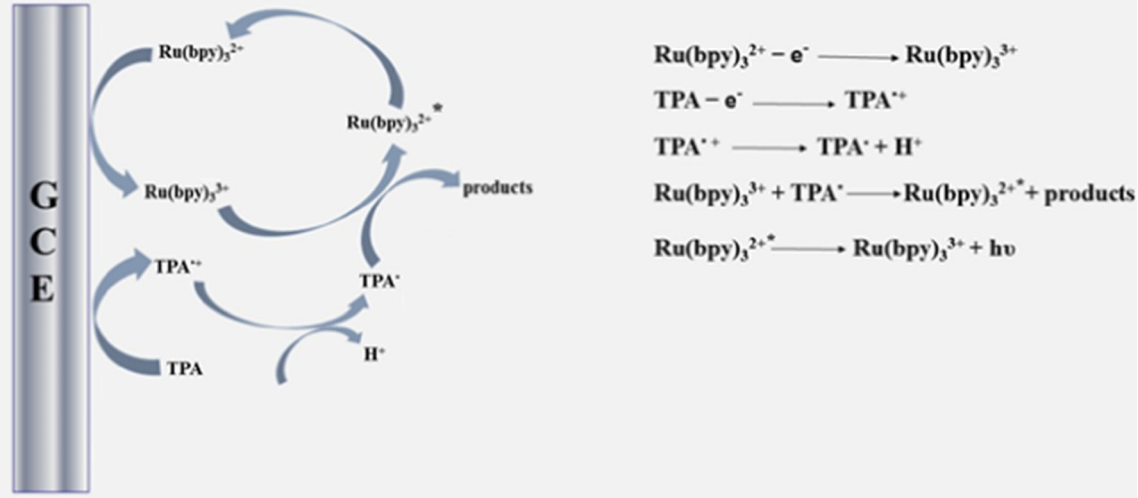

Scheme 2 Proposed mechanism of ECL sensor

concentration at the modified electrode as a result of the more excited state of $[Ru(bpy)_3^{2+}]^*$ produced with the increasing TPA concentration. The ECL intensity increased at 0.5 mM of TPA and decreased with further concentration of TPA.

The effect of scan rate (v) on ECL and CV signals of $Ru(bpy)_3^{2+}$/TPA systems was investigated (ESM Fig. S1(E)). The results showed that with increasing scan rate in the range between 25 to 100 mV/s the intensity of the ECL signal of $Ru(bpy)_3^{2+}$ increased and achieved the maximum value at 100 mV/s. At a lower scan rate, the formation of the intermediate is very slow, which causes a lower ECL intensity. At higher scan rates, shorter reaction time led immediately to lower concentration and smaller transmission of the reaction, resulting in a lower ECL intensity [41]. A scan rate of 100 mV/s was selected for further experiments because maximum ECL intensity was achieved for that scan rate.

ECL detection of Cyt C

Under the optimal experimental condition, the proposed sensor showed strong and stable ECL emission in the presence of TPA (Fig. 5a). However, the ECL intensities decreased dramatically by addition of Cyt C concentrations. The ECL sensor responses to different concentrations of Cyt C are illustrated in Fig. 5b. As shown, the ECL intensity decreased with an increase in the Cyt C concentrations in the range of 2.5 nM to 2 μM ($R = 0.995$, $n = 9$). The detection limit for Cyt C determination in this work was 0.7 nM (S/N = 3) and relative standard deviation (RSD) for the measurement of 10 nM Cyt C by six sensors was 4.4 %. Also, a comparative study was performed between the different reported analytical methods for the detection of Cyt C and this work. As shown in Table 1, the proposed Cyt C biosensor displays higher sensitivity, wider linear range, and lower detection limit than those of other analytical methods.

Interference studies were carried out by adding glucose, bovine serum albumin (BSA), arginine, and cysteine to the measuring solution of Cyt C in various concentrations. As

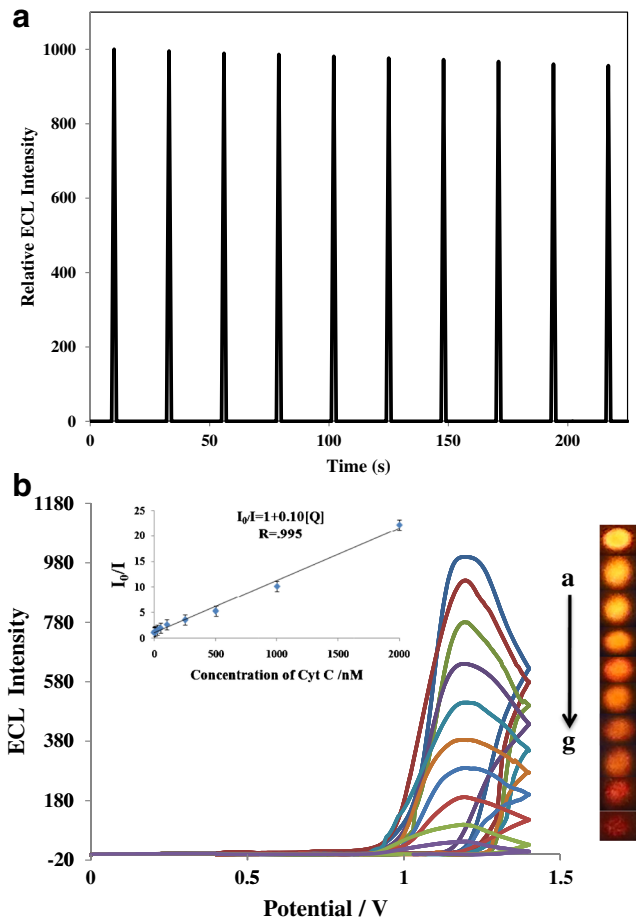

Fig. 5 **a** Stability of ECL signal from CeO_2-RGO/ $Ru(bpy)_3^{2+}$-CHIT modified electrode in 0.1 M pH 7.4 phosphate buffer solution, containing 0.5 mM TPA under ten cycles of CV scan. **b** Typical ECL signals of cytochrome *c* concentrations of samples were 0, 2.5, 5.0, 25, 50, 100, 250, 500, 1000, and 2000.0 nM (*a*–*g*, respectively)

Table 1 Comparison of the Cyt C biosensor with other reported methods

Analytical method	Detection limit	Linear range	Reference
Cyclic voltammetry	0.5 μM	1–1000 μM	[6
Cyclic voltammetry	10 nM	10 nM–500 μM	[4]
Amperometry	3.4 μM	1–600 μM	[42]
Fluorescence	0.41 μM	0.97–24 μM	[43]
Electrochemiluminescence	1.5 μM	4.0 to 324 μM	[10]
Electrochemiluminescence	0.7 nM	2.5–2000 nM	This work

shown in Fig. 6, no remarkable changes were observed compared to the quenching effect of Cyt C on ECL responses. Thus, the interference study results indicated that the biosensor has a good selectivity in the determination of Cyt C in real samples.

The applicability of the proposed sensor for the determination of Cyt C in human serum was examined. For this purpose, the plasma samples were diluted with pH 7.4 PBS to ensure that the concentrations were within the linear ranges of the method. Cyt C was spiked into the human serum samples. The results showed that the recoveries were in the range of 94–103 % and RSDs of 1.8–3.6 % (Table 2). The recoveries indicate that both the accuracy and repeatability of the proposed sensor are very satisfactory. It is very clear that the developed methodology has great potential for determination of Cyt C in complex biological matrixes.

Study of ECL quenching mechanism

A series of experiments were performed to study the ECL quenching of the $Ru(bpy)_3^{2+}$ /TPA system by Cyt C.

To verify whether Cyt C can interact with $Ru(bpy)_3^{2+}$ or TPA, we investigated the ECL of the $Ru(bpy)_3^{2+}$/Cyt C system without the presence of TPA (Fig. 7a). Curve a is related to the annihilation ECL mechanism of $Ru(bpy)_3^{2+}$[16]. It can be seen that Cyt C can also quench the ECL of $Ru(bpy)_3^{2+}$ in the absence of TPA (curve b). This result suggested that Cyt C most likely interacted directly with $Ru(bpy)_3^{2+}$. TPA here only acted as a co-reactant to enhance the ECL intensity of the system [44].

The fluorescence quenching was studied in the presence and absence of Cyt C. As shown in Fig. 7b, the fluorescence of $Ru(bpy)_3^{2+}$ with excitation at 350 nm and fluorescence emission peak at 620 nm could be quenched by Cyt C. The results showed that increasing the concentration of Cyt C resulted in a decrease in fluorescence emission of $Ru(bpy)_3^{2+}$. The fluorescence decrease of $Ru(bpy)_3^{2+}$ by Cyt C indicated that $Ru(bpy)_3^{2+}$ had a strong interaction with Cyt C [44].

Also, in order to know whether or not chemical reaction occurs between $Ru(bpy)_3^{2+}$and Cyt C, UV–visible absorption spectra of the $Ru(bpy)_3^{2+}$ Cyt C system were investigated. As shown in Fig. 7c, The $Ru(bpy)_3^{2+}$ shows absorption peaks at 286 and 455 nm (curve a). Cyt C had an absorption peak at around 410 nm (curve b). The absorption spectra of the mixed solution of the $Ru(bpy)_3^{2+}$-Cyt C were exactly the sum of that of the individuals (curve c). The results verify that no new compounds were produced by simply mixing Cyt C with $Ru(bpy)_3^{2+}$, which indicated that there is no chemical reaction between $Ru(bpy)_3^{2+}$ and Cyt C by simply mixing Cyt C with $Ru(bpy)_3^{2+}$ in the ground state [45]. Thus, the quenching of ECL signal by Cyt C can be due to the inhibitory effect of Cyt C on TPA (Scheme 2). Cyt C prevents the TPA from reaching the electrode surface which causes the decrease of the ECL intensity. Such behavior has been already reported by Wang et al. [13] and Hu et al. [10].

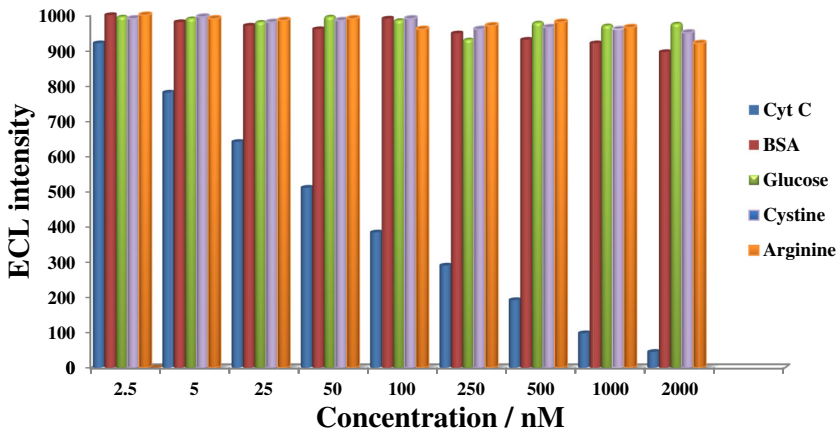

Fig. 6 Selectivity of the proposed ECL sensor in 0.1 M pH 7.4 phosphate buffer solution

Table 2 Recovery studies performed in spiked serum samples for applicability of the developed biosensor ($n = 3$)

Serum	Original (nmol L^{-1})	Added (nmol L^{-1})	Found (nmol L^{-1})	Recovery (%)	RSD (%, $n = 3$)
1	4.2	10	13.6	94	3.6
2	8.4	10	18.7	103	1.8
3	10.3	10	20.1	97	2.3

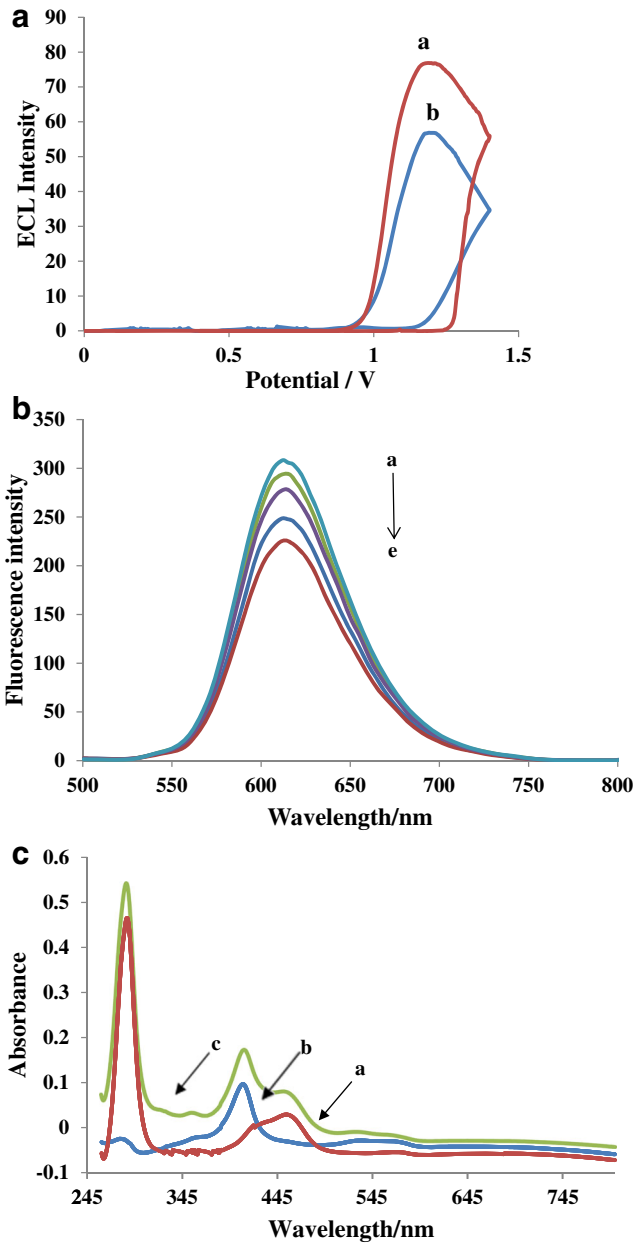

Fig. 7 **a** ECL of $Ru(bpy)_3^{2+}$ system without the presence of TPA. *a* 2.5 mM $Ru(bpy)_3^{2+}$, *b* 2.5 mM $Ru(bpy)_3^{2+}$ + 300 nM Cyt C. **b** Fluorescence intensity of 1×10^{-5} M $Ru(bpy)_3^{2+}$; Cyt C: 0, 25, 50, 75, 100 nm (*a–e*, respectively). **c** UV–visible absorption spectra for $Ru(bpy)_3^{2+}$ with Cyt C in 0.1 M pH 7.4 phosphate buffer solution *a* 2×10^{-7} M $Ru(bpy)_3^{2+}$, *b* 1×10^{-6} Cyt C, *c a* + b

The observed quenching behavior can be described by the Stern-Volmer equation: $F_0/F = 1 + K_{SV}[Q]$ where F_0 and F are the fluorescence intensities observed in the absence and presence of quencher, respectively. [Q] is the quencher concentration and K_{SV} is the Stern-Volmer quenching constant. The value of K_{SV} for ECL quenching of $Ru(bpy)_3^{2+}$ by Cyt C was calculated to be 1.1 nM .

Conclusions

In this work, a CeO_2NPs-RGO nanocomposite was prepared by a facile sonochemical method and used for making a novel ESL biosensor. This nanocomposite has large specific surface, good conductibility, and high stability that could provide a large active surface and promote the formation of radical species. The proposed CeO_2NPs-RGO/ $Ru(bpy)_3^{2+}$/ CHIT nanocomposite can enhance ECL intensity to provide a favorable initial ECL signal for construction of a quenching biosensor for detection of Cyt C. The proposed biosensor demonstrated its advantages of high sensitivity, selectivity, long-term stability, simple fabrication, and excellent specificity towards Cyt C. Therefore, this method has the ability to be extended for the detection of the protein in clinical analysis.

Acknowledgments The authors thank the Research Council of University of Tehran for financial support of this work.

Compliance with ethical standards All experiments with human plasma were also performed in compliance with the relevant laws in Iran and institutional guidelines, and relevant ethical committees in Tehran University of Medical Sciences and The University of Tehran approved the experiments. Consent was obtained for any experimentation with human subjects.

Conflict of interest The authors declare that they have no conflicts of interest.

References

1. Alleyne T, Joseph J, Sampson V. Cytochrome-c detection. Appl Biochem Biotechnol. 2001;90:97–105.
2. Brown GC, Borutaite V. Regulation of apoptosis bt the redox state of cytochrome c. Biochim Biophys Acta. 2008;177:877–881.

3. Loo FC, Ng SP, Wu CML, Konga SK. An aptasensor using DNA aptamer and white light common-path SPR spectral interferometry to detect cytochrome-c for anti-cancer drug screening. Sens Actuators B. 2014;198:416–23.
4. Fuku X, Iftikar F, Hess E, Iwuoha E, Baker P. Cytochrome c biosensor for determination of trace levels of cyanide and arsenic compounds. Anal Chim Acta. 2012;730:49–59.
5. Pandiaraj M, Benjamin AR, Madasamy T, Vairamani K, Aryad A, Kumar Sethyd N, et al. A cost-effective volume miniaturized and microcontroller based cytochrome c assay. Sens Actuators A. 2014;220:290–7.
6. Pandiaraj M, Madasamy T, Gollavilli PN, Balamurugan M, Kotamraju S, Rao VK, et al. Nanomaterial-based electrochemical biosensors for cytochrome c using cytochrome c reductase. Bioelectrochemistry. 2013;91:1–7.
7. Ocaña C, Lukic S, del Valle M. Aptamer-antibody sandwich assay for cytochrome c employing an MWCNT platform and electrochemical impedance. Microchim Acta. 2015;182:2045–53.
8. Ocaña C, Arcay E, del Valle M. Label-free impedimetric aptasensor based on epoxy-graphite electrode for the recognition of cytochrome c. Sens Actuators B. 2014;191:860–5.
9. Liao D, Chen J, Li W, Zhang Q, Wang F, Li Y, et al. Fluorescence turn-on detection of a protein using cytochrome c as a quencher. Chem Commun. 2013;49:9458–60.
10. Hu XW, Mao CJ, Song JM, Niu HL, Zhang SY, Huang HP. Fabrication of GO/PANi/CdSe nanocomposites for sensitive electrochemiluminescence biosensor. Biosens Bioelectron. 2013;41:372–8.
11. Shamsipur M, Molaabasi F, Hosseinkhani S. Detection of early stage apoptotic cells based on label-free Cytochrome c assay using bioconjugated metal nanoclusters as fluorescent probes. Anal Chem. 2016;88:2188–97.
12. Yin X, Cai J, Feng H, Wu Z, Zou J, Cai Q. A novel VS_2 nanosheet-based biosensor for rapid fluorescence detection of cytochrome c. New J Chem. 2015;39:1892–8.
13. Wang T, Zhang S, Mao C, Song J, Niu H, Jin B, et al. Enhanced electrochemiluminescence of CdSe quantum dots composited with graphene oxide and chitosan for sensitive sensor. Biosens Bioelectron. 2012;31:369–75.
14. Miao WJ. Electrogenerated chemiluminescence and its biorelated applications. Chem Rev. 2008;108:2506–53.
15. Hu L, Xu G. Applications and trends in electrochemiluminescence. Chem Soc Rev. 2010;39:3275–304.
16. Wei H, Wang E. Solid-state electrochemiluminescence of tris(2,2′-bipyridyl) ruthenium. TrAC Trend Anal Chem. 2008;27:447–59.
17. Xiong C, Wang H, Yuan Y, Chai Y, Yuan R. A novel solid-state $Ru(bpy)_3^{2+}$ electrochemiluminescence immunosensor based on poly(ethylenimine) and polyamidoamine dendrimers as co-reactants. Talanta. 2015;131:192–7.
18. Lei J, Ju H. Signal amplification using functional nanomaterials for biosensing. Chem Soc Rev. 2012;41:2122–34.
19. Borghei YS, Hosseini M, Dadmehr M, Hosseinkhani S, Ganjali MR, Sheikhnejad R. Visual detection of cancer cells by colorimetric aptasensor based on aggregation of gold nanoparticle induced by DNA hybridiztion. Anal Chim Acta. 2016;904:92–7.
20. Ahmadzadeh KH, Hosseini M, Dadmehr M, Ganjali MR. Rapid restriction enzyme free detection of DNA methytransferase activity based on DNA-templated siver nanoclusters. Anal Bioanal Chem. 2016;408:4311–8.
21. Novoselov KS, Geim AK, Morozov SV, Jiang D, Zhang Y, Dubonos SV, et al. Electric field effect in atomically thin carbon films. Science. 2004;306:666–9.
22. Pumera M. Graphene-based nanomaterials and their electrochemistry. Chem Soc Rev. 2010;39:4146–57.
23. Hosseini M, Mirzanasiri N, Rezapour M, Sheikhha MH, Faridbod F, Norouzi P, et al. Sensitive determination of carbidopa through the electrochemiluminescence of luminol at graphene-modified electrodes. Luminescence. 2015;30:376–81.
24. Peng S, Zou G, Zhang X. Nanocomposite of electrochemically reduced graphene oxide and gold nanoparticles enhanced electrochemilunescence of peroxydisulfate and its immunosensing abililty towards human IgG. J Electroanal Chem. 2012;686:25–31.
25. Zhou K, Zhu Y, Yang X, Li C. Preparation and application of mediator-free H_2O_2 biosensors of graphene-Fe_3O_4 composites. Electroanalysis. 2011;23:862–9.
26. Sun C, Li H, Chen L. Nanostructured ceria-based materials: synthesis, properties, and applications. Energy Environ Sci. 2012;5:8475–505.
27. Zhang M, Yuan R, Chai Y, Wang C, Wu X. Cerium oxide-graphene as the matrix for cholesterol sensor. Anal Biochem. 2013;436:69–74.
28. Zhu S, Guo J, Dong J, Cui Z, Lu T, Zhu C. Sonochemical fabrication of Fe_3O_4 nanoparticles on reduced graphene oxide for biosensors. Ultrason Sonochem. 2013;20:872–80.
29. Dezfuli AS, Ganjali MR, Norouzi P, Faridbod F. Facile sonochemical synthesis and electrochemical investigation of ceria/graphene nanocomposites. J Mater Chem B. 2015;3:2362–70.
30. GeorgakilasV KN, Kemp KC, Hobza P. Functionalization of graphene: covalent and non-covalent approaches, derivatives and applications. Chem Rev. 2012;112:6156–214.
31. Wu ZS, Zhou G, Yin LC, Ren W, Li F, Cheng HM. Graphene/metal oxide composite electrode materials for energy storage. Nano Energy. 2012;1:107–31.
32. Teymourian H, Salimi A, Khezrian S. Fe_3O_4 magnetic nanoparticles/reduced graphene oxide nanosheets as a novel electrochemical and bioeletrochemical sensing platform. Biosens Bioelectron. 2013;49:1–8.
33. Jafari S, Faridbod F, Norouzi P, Dezfuli AS, Ajloo D, Mohammadipanah F, et al. Detection of Aeromonas hydrophila DNA oligonucleotide sequence using a biosensor design based on ceria nanoparticles decorated reduced graphene oxide and fast Fourier transform square wave voltammetry. Anal Chim Acta. 2015;895:80–8.
34. Wang G, Bai J, Wang Y, Ren Z. Prepartion and electrochemical performance of a cerium oxide–graphene nanocomposite as the anode material of a lithium ion battery. Scr Mater. 2011;65:339–42.
35. Srivastava M, Kumar Das A, Khanra P, Elias Uddin M, Kim NH, Hee Lee J. Characterizations of in situ grown ceria nanoparticles on reduced graphene oxide as a catalyst for the electrooxidation of hydrazine. J Mater Chem A. 2013;1:9792–801.
36. Hosseini M, Moghaddam MR, Faridbod F, Norouzi P, Karimi Pur MR, Ganjali MR. A novel solid-state electrochemiluminescence sensor based on a $Ru(bpy)_3^{2+}$/nano Sm_2O_3 modified carbon paste electrode for the determination of L-proline. RSC Adv. 2015;5:64669–74.
37. Hosseini M, Karimi Pur MR, Norouzi P, Moghaddam MR, Faridbod F, Ganjali MR, et al. Enhanced solid-state electrochemiluminescence of $Ru(bpy)_3^{2+}$ with nano-CeO_2 modified carbon paste electrode and its application in tramadol determination. Anal Methods. 2015;7:1936–42.
38. Hong LR et al. Highly efficient electrogenerated chemiluminescence quenching of PEI enhanced $Ru(bpy)_3^{2+}$ nanocomposite by hemin and Au@CeO_2 nanoparticles. Biosens Bioelectron. 2015;63:392–8.
39. Zhu Y, Li G, Zhang SY, Song JM, Mao CJ, Niu HL, et al. Synthesis and electrochemiluminescence of the CeO_2/TiO_2 composite. Electrochim Acta. 2011;56:7550–4.
40. Zhou L, Huang J, Yang L, Li L, You T. Enhanced electrochemiluminescence based on $Ru(bpy)_3^{2+}$-doped silica nanoparticles and graphene composite for analysis of melamine in milk. Anal Chim Acta. 2014;824:57–63.
41. Noffsinger JB, Danielson ND. Generation of chemiluminescence upon reaction of aliphatic amines with tris(2,2′-bipyridine)ruthenium(III). Anal Chem. 1987;59:865–8.

42. Tan S, Hua L. Amperometric detection of cytochrome c by capillary electrophoresis at a sol–gel carbon composite electrode. Anal Chim Acta. 2001;450:263–7.
43. Zhang W, He X, Chen Y, Li W, Zhang Y. Composite of CdTe quantum dots and molecularly imprinted polymer as a sensing material for cytochrome c. Biosens Bioelectronics. 2011;26:2553–58.
44. Qiu B, Jiang XF, Guo LH, Lin ZY, Cai ZW, Chen GN. A highly sensitive method for detection of protein based on inhibition of $Ru(bpy)_3^{2+}$/TPrA electrochemiluminescent system. Electrochim Acta. 2011;56:6962–5.
45. Huang B, Zhou X, Xue Z, Wu G, Du J, Luo D, et al. Quenching of the electrochemiluminescence of Ru(bpy)(3)(2)(+)/TPA by malachite green and crystal violet. Talanta. 2013;106:174–80.